KERNFORSCHUNGSZENTRUM

KARLSRUHE

März 1977 KFK 2389

Institut für Reaktorentwicklung
Projekt Schneller Brüter

Sodium Boiling Experiments in an Annular Test Section under Flow Rundown Conditions

A. Kaiser, W. Peppler

GESELLSCHAFT
FÜR
KERNFORSCHUNG M.B.H.

KARLSRUHE

GESELLSCHAFT FÜR KERNFORSCHUNG M.B.H.

KARLSRUHE

KERNFORSCHUNGSZENTRUM KARLSRUHE

KFK 2389

Institut für Reaktorentwicklung

Projekt Schneller Brüter

Sodium Boiling Experiments in an Annular Test Section under Flow Rundown Conditions

A. Kaiser
W. Peppler

Gesellschaft für Kernforschung mbH Karlsruhe

Summary

Experiments have been carried out using sodium in an annular test section geometry to simulate boiling development in a fast reactor core under the somewhat improbable conditions of primary circulator pump run-down with coincidental failure of the reactor trip system.

Induction heating of the outer tube was used, the axial heat flux distribution being linear. Boiling was achieved by means of a steady reduction of the coolant flow from normal steady state values, heat fluxes being appropriate to reactor conditions. Boiling was allowed to continue until indications of permanent dryout of the heated tube were received, at which stage power was terminated to prevent damage to the test section.

The results obtained provide useful information on the transient development of boiling, the axial distribution of void within the channel, initial superheat, liquid film thickness, dryout and rewetting. The experiments thus provide a source of data against which computer codes such as BLOW3, based on theoretical models of boiling may be validated.

Natrium-Siedeexperimente in einer Ringkanal-Teststrecke zum Kühlmittel-Störfall

Zusammenfassung

Zur Simulation von Siedevorgängen in einem Brennelement eines schnellen, natriumgekühlten Reaktors unter der Annahme eines Pumpenabfalls bei gleichzeitigem Versagen der Schnellabschaltung des Reaktors wurden Versuche mit Natrium in Ringkanal-Geometrie durchgeführt. Die Beheizung erfolgte induktiv über das Außenrohr der Teststrecke (lineare Verteilung).

Ausgehend von stationären Bedingungen wurde das Sieden durch lineare Reduktion des Kühlmitteldurchsatzes auf Null eingeleitet. Die Leistung wurde abgeschaltet, sobald sich durch anhaltende lokale Austrocknung des Kühlkanals eine Gefahr durch Überhitzung der Teststrecke ergab.

Die Versuchsergebnisse liefern Informationen über den zeitlichen Ablauf der Siedevorgänge, die axiale Ausdehnung des leergesiedeten Bereichs, Siedeverzüge, Restfilmstärken auf der Heizfläche und Wiederbenetzung nach vorangegangener Austrocknung. Die Ergebnisse dienten außerdem zur Überprüfung des Rechenprogramms BLOW3, einem auf den Vorstellungen des Mehrblasensiedens basierenden, eindimensionalen Modell.

Contents

1. Introduction

The experiments reported in this paper form a small part of a major experimental program designed to study the processes involved in the boiling of the liquid metal coolant in a fast reactor. Such boiling can be initiated under a variety of circumstances, which in terms of their probability and severity of potential consequences pose safety hazards of varying degrees to reactor safety. For reviews of the reactor safety implications and the experimental program as a whole, the reader is referred to Refs. 1 and 2.

The particular experiments reported here were performed in an attempt to represent the unlikely event of a loss of electrical supplies to the primary circulatory pumps of a fast reactor coincident with a failure of the reactor to trip. The experiments give an idea of the spatial and temporal development of boiling events, and serve as a source of data against which computer models of sodium boiling, such as the BLOW3 code [1] can be validated. This code, which is based on a multibubble one dimensional concept of boiling, and which embodies the results of previous boiling experiments [3], calculates the voiding pattern in fast reactor subassemblies under loss of flow conditions.

The experiments were performed in annular channel geometry with induction heating. A further step towards a more realistic simulation of reactor subassembly hydraulic conditions is to be found in the analogous experiments which have recently been performed using an electrically heated seven pin bundle [4].

2. Problems in the Simulation of Reactor Conditions

The boiling process under flow rundown conditions is mainly influenced by the parameters axial temperature distribution, system pressure, flow rundown characteristic and flow resistances. By appropriate selection of the test parameters and the pump rundown characteristic, axial temperature distributions were generated which, at the onset of boiling were similar to those calculated for the SNR reactor transient. This is of considerable significance for boiling development.

The deviations from the exact reactor conditions were mainly due to the power distribution(chopped cosine cf. linear), the heat capacity (fuel rod/nickel tube), the pressure drop, and the heated length (fuel element 950 mm, test section 500 mm). For technical reasons only a 500 mm section could be heated in the experiment. This was taken into consideration by raising the sodium temperature at the inlet of the test section. The hydraulic diameters (fuel element subchannel d_h = 5,4 mm and test section d_h = 4 mm) are comparable.

A major influence on the movement of liquid columns during boiling pulsations is exerted by the flow resistances. Due to the low delivery head of the pump the pressure drop Δp across the test section (including the throttling valve) was limited to a maximum value of $2 \cdot 10^5$ Pa*. Consequently, it was below the SNR value applicable between the lower and the upper plenum (see Table 1).

The maximum deviation in the flow resistances of fuel elements and test setup was found in the zone preceding the point of onset of boiling, i.e., within the zone of single-phase flow. The pressure drop in the fuel element inlet alone amounts to about $2.5 \cdot 10^5$ Pa*.

---

* 10^5 Pa = 1 bar

3. Setup and Conduct of Experiments

3.1 Test Section and Instrumentation

The test section (Fig. 1) consisted of an induction heated nickel tube of 12 mm/9 mm diameter and 500 mm length. In its interior a hollow displacement tube of 5 mm outer diameter was placed concentrically which extended between the lower and upper flowmeters (D1 and D2). The test section was installed in the sodium boiling loop (NSK) of the Institut für Reaktorentwicklung without a bypass.

Six thermocouples of 0.5 mm Ø were soldered into the heated tube such that the points of measurement lay in line at 0.8 mm distance from the inner surface. Additional thermocouples recorded the sodium temperatures and tube wall temperatures at the positions of the various measurement devices (flowmeters, pressure transducers, bubble detectors).

The flow velocities indicated in the diagrams of this report always relate to the annular channel cross-section of the test section. The signals of the flowmeter DF and of the bubble detectors (Jodel principle) X and Y served to follow the time-dependent axial development of the liquid/vapor interface downstream of the heated section during boiling. The arrangement of a bubble detector is represented schematically in Fig.2. A constant direct current of about 40 mA was passed across the test section between the two electrodes, the tube being normally filled with sodium. If the sodium in the tube was displaced by a vapor bubble at the point of measurement, the electric resistance and hence the potential difference was increased (see also Section 4.1 and Fig.11).

By means of a Barton cell the static pressure p_o was recorded in the inlet zone of the test section while the pressure pulsations during boiling were recorded by three piezoelectric pressure transducers.

3.2 Recording of Measured Values

The measured values were digitized and stored on magnetic tape by a central electronic data acquisition system. The sampling frequency was 500 Hz. During each cycle, flow and pressure signals were recorded eight times, yielding for these parameters an effective sampling frequency of 4000 Hz. At the same time, the most important signals were recorded by a UV-recorder allowing a rapid survey of the development of the test.

3.3 Simulation of Pump Rundown

Based on a steady-state condition characterized by a constant energy supply, and with initial flow velocities in the range 3 to 5 m/s the coolant flow rate was lowered by linear reduction of the voltage supply to an electromagnetic pump. This reduction was achieved by means of a servo motor. The development over time of the velocity v_2 and of the temperature T_i at the upper end of the heated section have been represented for 6 selected tests in Figs. 3 and 4. For comparison, the development of the average coolant velocity calculated for an SNR fuel element (as of September 1974) is illustrated in the central section of Fig. 4.

3.4 Parameter Variation

Table 2 contains a survey of the variation of test parameters for all the 13 experiments performed. The pressure development in the test section depended on the flow and on the selected cover gas pressure in the expansion tank (0.785, 1.18 and $1.57 \cdot 10^5$ Pa). The heat flux was varied in 5 steps (99, 123, 149, 180 and 213 W/cm^2).

For a comparison with SNR a rather more appropriate parameter than the heat flux is the power per unit volume of coolant channel, P_v, indicated in Table 2. In the central SNR fuel element this has an average value of 1130 W/cm^3. The last two columns give an indication of the flow reduction up to the onset of boiling.

4. Test Evaluation and Results

4.1 Boiling Characteristic

Figs. 5 to 10 illustrate transient records of the most important signals, along with the void development and accelerational pressure drop deduced from these measurements.

v_1, v_2 : Flow velocities at the inlet and at the outlet of the heated section (times of flow reversal see Table 3).

s_1, s_2 : Axial position of vapor/liquid interfaces.

Δp_{dyn3} : Dynamic pressure measured 40 mm downstream of the heated length.

Δp_u : Pressure difference between the vapor zone and the gas plenum of the expansion tank acting on the upper sodium column. It was calculated by Eq. (7) in [3] (p. 30) taking into account the fluid friction, the mass inertia and the geodetic height of the sodium column (see Eq. (1) p.8).

T_i, T_n, T_o (partial): Wall temperatures in the heated part of the test section.

T_g : Sodium temperature 70 mm downstream of the heated part of the test section.

In addition, the results of calculations using the BLOW 3 model are indicated for the runs No. 16/20 (Fig. 6) and 16/23 (Fig. 8) (more details are given in Section 4).

The boundaries of the boiling region traced in the diagrams were determined by integration of the velocities v_1 and v_2 taking into account signals from the bubble detectors X and Y, the flowmeter DF and different wall and sodium temperature readings. This procedure will be described now using Fig. 11.

The times at which the Jodel signals indicated the change from the "filled" to the "empty" conditions were projected onto the integrated flow signal $\int v_2 dt$. These formed fixed points through which the upper phase boundary, represented by $\int v_2 dt$, must pass.

No bubble detector was available to determine the lower phase boundary. The control points were given by discontinuities in the rate of change of temperature in the tube wall, e.g., hold-up phases indicate evaporation of the liquid film, and very steep positive temperature gradients can be assumed to be caused by condensation processes on voided,still subcooled surfaces.

It appears from the patterns of initial boiling development that the boiling process in the individual experiments did not begin in a uniform way. Usually, a small initial boiling superheat led to the formation of individual bubbles of minor size. These bubbles recorded both by the flowmeter and by the dynamic pressure transducers could not always be located very accurately because of their small axial extension.

The rate of bubble growth can be deduced firstly from the inlet and outlet flow velocities. It is essentially governed by the pressure in the vapor, a measure of which may be obtained from the dynamic pressure transducers (e.g. Δp_{dyn3}). On the other hand, the pressure development depended on the temperature distribution before the onset of boiling: the higher the initial superheat and the larger the superheated region the stronger was the ejection of sodium both upwards and downwards (e.g. run No. 16/23, Fig. 8). More about this connection will be given in Section 4.2 (see below). But now some more characteristics observed during the boiling process together with conclusions will be reported.

The later stages of the experiments were uniformly marked by oscillations of the upper and the lower sodium columns, accompanied by corresponding oscillations in flow, pressure and temperature, and hence also in net evaporation and condensation rates. The fact that in these oscillations the upper phase boundary with its greater amplitudes penetrated much further into the unheated part of the test section than the lower phase boundary can be attributed to the lower temperature of the bottom part of the test section at the onset of boiling and to

the higher inertia and frictional resistance of the whole circuit section preceding the boiling zone.

Applying the graphical method to evaluate the boundaries of the boiling region, as explained earlier, the passage of liquid slugs through the vapor zone can be observed during the boiling process. On the one hand, the departure of masses of liquid was recorded at the lower phase boundary as a result of the formation of new bubbles while, on the other hand the arrival of additional liquid was recorded at the upper liquid column at the times of deepest penetration into the vapor zone. This coming together of liquid masses was indicated by sharp pressure peaks (see e.g. Δp_{dyn3}). However, it can be concluded from the individual temperature plots that the slugs did not in all cases occupy the total coolant channel cross-section when they moved upwards through the voided zone.

The large axial temperature gradients prevailing in the test section at the onset of boiling (e.g. Fig. 5) were rapidly reduced by boiling events. This was initially due to the downward movement of the lower sodium column and later to the very efficient energy transfer which can be achieved by interphase mass transfer processes. During this stage temperatures in the upper part of the heated section generally rose because of power still being applied. An exception was run No. 16/23 (Fig. 8). The temperatures in the upper part decreased for about 1 s after the onset of boiling. This case was marked by a particularly high superheat of about 90 ^{o}C at the end of the heated section, and the fall in temperature is attributed to high evaporation rates which efficiently dissipated this stored energy.

4.2 Initial Boiling Superheat

As already mentioned boiling started in most of the tests with the formation of several individual bubbles before large scale ejection took place and subsequently the two-phase boundaries remained separated till the end of the boiling process. At the times at which the formation of new bubbles was indicated, the axial temperature distribution along the inside wall of the heated part of the test section has been plotted in Figs. 12 to 17 together with the saturated vapor temperatures calculated from the local pressure. The temperatures of the inside walls were obtained from the logarithmic radial temperature distribution by extrapolation of the values measured in the

walls while the pressures were derived from the output of the pressure transducer PO taking into account the geodetic level and frictional flow losses. The initial boiling superheats contained in Table 3 (the last but second column) have been taken from these diagrams. No values are given in the table for cases in which the point of bubble formation was not unambiguously determined by signals from the bubble detectors and thermocouples.

The fact that the flowmeters and pressure transducers indicated boiling in some cases even though the inner wall temperatures where boiling was believed to occur were below the saturation temperature, indicates that there was probably an eccentricity of the displacement body relative to the outer tube. This eccentricity would result in differential coolant heating with azimuthal temperature gradients. The short lifetime of the individual bubbles indicates a relatively small overheated region within a predominantly still subcooled environment.

To overcome the above mentioned difficulty in the direct measurement of initial boiling superheat by means of thermocouples, another method of estimating the amount of superheat in the region of boiling initiation was applied: this utilized the pressure drop Δp_u already mentioned in the preceding section. The pressure acting as a resultant on the lower end of the upper sodium column is calculated according to the following equation:

$$\Delta p_u = \rho \cdot \{v_2^2(k_1(1-s_2) - k_2) + \frac{dv_2}{dt}(1-s_2) + g(h-s_2)\} \qquad (1)$$

where k_1, k_2 are constants determined by the channel geometry and the friction coefficients,

v_2 is the velocity of the upper sodium column,

s_2 is the location of the interface,

$\frac{dv_2}{dt}$ is the acceleration of the upper sodium column,

ρ is the density of the sodium,

$1-s_2$ is the residual length of the annular coolant channel downstream of s_2,

$h-s_2$ is the level difference between s_2 and the free sodium level in the expansion tank.

In this equation the friction and acceleration losses in the tubes (nominal width 25 and 50 mm, respectively) at and above the flow-meter D2, respectively, were neglected because of the much lower coolant velocity there.

Assuming that the bubble during the first phase of growth was in thermodynamic equilibrium with the film surface, the pressure rise can be obtained from the vapor pressure corresponding to the temperature of the overheated film or of the inner wall, respectively, to a first approximation. So, the initial boiling superheats can be determined from the pressure difference Δp_u (according to Eq. (1)) and the absolute pressure p_s at the point of bubble formation from the table of vapor pressure data for saturated sodium.

In Eq. (1) the acceleration dv_2/dt is normally the dominant term. Within the first milliseconds after bubble formation the change in velocity was small and consequently did not yield relevant values for initial boiling superheat. So, the boiling superheats ΔT_s indicated in the next to last column of Table 3, refer to the time (see last column) of the maximum positive velocity change during the phase of bubble growth. Application of this method does not result in an exact value of superheat immediately at the point and for the time of boiling initiation. But, if one takes into account the calculated temperature rise of the wall of about 60...90 K/s (due to the power still applied) within the above mentioned time period during the phase of bubble growth one gets a rather good approximate value for the superheat occurred.

4.3 Residual Film Thickness

After the coolant has been expelled and also after the passage of liquid slugs, a sodium film obviously remains on the coolant channel walls. For some period of time this film cooled the heated wall by evaporation. This is clearly indicated by the records of transient temperature development in the wall. Before the local disappearance of the sodium film, which is made apparent by the occurrence of a temperature rise in the uncooled wall, three different types of temperature courses were observed at the tube wall. Taking run No. 16/20 as an example these observations together with some deductions will be described in the following (compare Figs. 6 and 11):

1. The temperature of the inner wall was above the local saturated vapor temperature. Therefore the tube temperature fell at the onset of boiling (T_i from t = 7.05 ... 7.20 s).

2. The temperature at the inner wall approximately corresponded to the saturated vapor temperature. A distinct phase of constant temperature (T_k from 7.10 ... 7.25 s) was observed during which heat input and energy loss by evaporation were roughly equal.

3. The temperature at the inner wall was below the saturated vapor temperature. Under these conditions such a region became a condensation zone within the vapor bubble, which could be recognized from a characteristically extremely steep temperature rise (e.g. T_m from 7.07 ... 7.22 s). This rise exceeded that of an uncooled wall heated continuously. Only when a temperature corresponding to the local saturation temperature was exceeded, did a boiling phase follow during which the film evaporated (cf. T_m from 7.22 ... 7.31 s).

To clarify some details of these events transient calculations were performed with the TIGER program [5]. For this an axial section of 10 mm length in the heated zone of the test section was considered (see Fig. 18) which was divided into several concentric radial zones (nodes 1 to 7). The displacement body was not included in the calculation. The center of node 3 corresponds to the location of the thermocouples (e.g. T_i). The total power input was generated in the outermost ring (node 1) for the sake of simplicity, and this was essentially in line with the experimental conditions (high frequency principle). The node 8 adjoined the inside tube surface and served as a heat sink (evaporation film). Since TIGER cannot calculate evaporation, the heat transfer coefficient between nodes 7 and 8 was given a very high value. Axial heat conduction was neglected in the calculation since radial temperature gradients were much greater than the axial gradients and the wall thickness was small compared to the axial dimensions. The result of two of these calculations is represented in Fig. 19 for the main boiling phase of run No. 16/14. The computation called for a certain amount of iteration since the film temperature (node 8), which is, strictly speaking, unknown , was an input value and the measured temperature T_i an output value. The calculation began at the moment at which the film was left on the tube wall (either by ejection or rewetting). Loss of heat transfer

at the time of dryout was represented by setting the heat transfer coefficient to zero. Immediately afterwards the inner wall temperature (T_7) increased steeply. The temperature of node 3 increased in a way that corresponds to heat generation and heat capacity of an uncooled tube.

Also plotted in Fig. 19 is the saturation temperature corresponding to the pressure which was estimated by use of Eq. (1). The fact that during the periods in which the tube wall was obviously cooled, its temperature was always above this saturation temperature confirms the assumption that cooling was a result of film evaporation. Re-wetting of the dried tube wall was a result in some cases of the pulsating of the upper sodium column (e.g. T_i, Figs. 8 and 9), in other cases of liquid droplets separating from the lower phase boundary during boiling and being transported upwards by the vapor flow (e.g. T_n in Figs. 5, 9 and 10).

As well as for the observed evaporation processes calculations with the TIGER code could be done for the condensation processes (see point 3 of the above mentioned types of temperature courses). But they were of less interest in this context.

The main objective of the TIGER calculations done was the estimation of the so-called effective film thickness S_{eff} by means of the heat flux obtained from these calculations. This film thickness, the evaporation of which brought about wall cooling, can be calculated by the following heat balance:

$$\int q\,dt = S_{eff} \cdot \rho \cdot r \qquad (2)$$

The left hand side of Eq. (2) represents the energy per unit area released by the inner pipe wall surface obtained from the integration of the heat flux in Fig. 17. The right hand side is the mean heat of evaporation per unit area of a liquid layer of the thickness S_{eff} within the time period of the integration. The effective film thickness so determined will in only very rare cases agree with the amount remaining on the tube wall immediately after removal of the liquid phase. Changes in the film thickness can be due both to the deposition of droplets from the vapor flow and to shear forces acting on the film as a result of the more rapid vapor flow. Four film thicknesses calculated from Eq. (2) have been entered in Table 4.

For these and other cases the effective film thickness was also calculated by an approximate method based on an energy balance. The evaporation energy calculated as the sum of the reduction in the stored energy of the nickel test tube and the energy added to the test section by power input is represented by:

$$r \cdot \rho \cdot S_{eff} = c_{pNi} \cdot \frac{m_{Ni}}{A} \cdot \Delta T + q \cdot \Delta t \qquad (3)$$

The time interval Δt was determined by the periods between successive maxima and minima of the measured temperature in the tube wall ($dT/dt = 0$); ΔT is the temperature reduction during Δt.

It appears from Table 4 that the values obtained by this approach agree very well with those obtained by the much more demanding method using TIGER, and give a spectrum of film thicknesses from 0.05 to 0.18 mm.

In earlier experiments [3] values between 0.014 and 0.114 mm were measured after primary ejection. Fauske [6] indicates values for the residual liquid fraction which under reactor conditions correspond to film thicknesses between 0.1 and 0.2 mm. Spiller [7] indicates initial values of 0.08 mm on average.

Scattering of film thicknesses in the experiments performed in test section No. 16 as well as in earlier experiments [3] is not so much due to the somewhat coarser mode of calulation but rather to the statistical character of the local and time dependent interaction between the liquid film and the vapor flowing over it.

4.4 Boiling Frequency Analysis

The frequency analysis of signals of the piezo-quartz pressure transducers during boiling did not yield the expected results. The cross-correlation of the signals of the dynamic pressure transducers between each other and with flow meter signals showed reasonable agreement only for the single bubble frequency (5...15 Hz) and the oscillations of the sodium columns during the main boiling phase. No satisfactory conclusion could be reached at higher frequencies. From the fact, that the auto-power spectral densities of the pressure signals showed quite

different dominating frequencies it is deduced that the pressure signals were influenced strongly by the natural frequencies of the measuring devices. The poor results of this investigation does not justify the appearance of a figure in this report.

5. Verification of Experiments Using BLOW 3

Two of the experiments have been verified by Wirtz [1] using the BLOW 3 computer model (see Figs. 6 and 8).

In the test which produced the maximum initial boiling superheat (Fig. 8, run No. 16/23) pulsation of the upper sodium column after the onset of boiling is very well represented in amplitude and frequency. However, this agreement is completely missing for the lower phase boundary. Wirtz [1] explains this disagreement that has been found as being a systematic difficulty, by the fact that his model based on reactor conditions (parallel coolant channels with constant pressures in the lower and in the upper plenum) cannot adequately represent the conditions found in the test circuit upstream of the heated zone.

The agreement between the calculation and the experiment is not good in the second case (Fig. 6, run No. 16/20) for either the lower or the upper phase boundaries. In this case, where only a moderate initial boiling superheat occurred, the disagreement of the movement of the upper sodium column may be due to some irregularities in the test procedure pointed out in the following. The onset of boiling was followed by a short period of quiescent boiling (t = 7.2 ... 7.4 s) with only slight pressure variations, during which the upper end of the heated zone was completely uncooled. Consequently, in this test, excessive temperatures were reached relatively quickly, which resulted in early termination of power supply. A comparison of temperatures T_l (not marked in the diagrams) with T_k indicates that in this experiment too, there was non-uniform heating of the test section in the azimuthal direction during the transient phase. The BLOW 3 program is not capable by its conception to deal with such irregularities.

So, one can state that only that part of the experiments with symmetrical heating of the coolant channel is suited to be calculated with the BLOW 3 code. In the meantime the model of the code was improved considerably, so that the above discussed calculations should be regarded as very preliminary.

6. Conclusions

Using single channel geometry as in these experiments it is not possible to model exactly all the important geometric and thermal-hydraulic characteristics of a fast reactor fuel bundle. Also, it is not possible to obtain the effects of reactivity feedback (e.g. from Doppler or from void reactivity) which would be found in a real reactor. Such sophistication may be obtained only in in-pile experiments or in advanced theoretical models. In spite of these deficiencies the experimental results give valuable insight into the development of the boiling processes under these particular conditions.

The main deductions which can be made from the experimental results are as follows:

- Previous results [3] for the case of total loss of cooling under inlet blockage conditions were largely confirmed.

- Under pump rundown conditions with low superheat, boiling generally started with small bubbles, which recondensed completely. The later stages of boiling in these cases, as well as in the cases of large superheat, were marked by large oscillations of the vapor volume without complete condensation

- During this oscillatory boiling, liquid slugs were transported upwards from the lower void boundary. These slugs became subdivided thereby forming an unsteady two-phase flow.

- The amount of liquid which continued to be fed into the test section by residual pump head after the onset of boiling does not greatly influence the course of the boiling process. This is confirmed by the fact that after voiding of the lower part of the test section, in most cases excessive increases in temperature there led to power shut-off.

- Initial boiling superheats up to 53 K were observed.

- The evaluated effective local film thicknesses lay in the range 0.05 to 0.15 mm. This demonstrates once more the statistical nature of transient boiling processes.

7. Nomenclature

A	m^2	area
c_p	J/kg K	specific heat
d_h	mm	hydraulic diameter
g	m/s^2	acceleration due to gravity
h	m	height
k_1	$\frac{1}{m}$	constant
k_2	-	constant
l	m	length
m	kg	mass
P_v	W/cm^3	power per unit volume
p	Pa	pressure
q	W/cm^2	heat flux
r	J/kg	latent heat of evaporation
S	mm	film thickness
s	m	axial coordinate of two-phase interface
T	^oC	temperature
ΔT_s	K	initial boiling superheat
t	s	time
v	m/s	sodium velocity
ρ	kg/m^3	density

Indices

dyn	dynamic
eff	effective
G	cover gas
Ni	nickel
s	boiling
u	upper sodium column
w	wall

8. Literature

/1/ P. Wirtz:
Ein Beitrag zur theoretischen Beschreibung des Siedens unter Störfallbedingungen in natriumgekühlten schnellen Reaktoren. KFK 1858 (Oktober 73)

/2/ K. Gast, W. Peppler, D. Smidt:
Sodium Boiling Experiments and their Importance for the Reactor Safety. Proc. of the Fast Reactor Safety Meeting April 2-4, 1974, Beverly Hills, Calif.
Conf. -740401- P3

/3/ W. Peppler:
Experimentelle Untersuchungen der Siedevorgänge mit Natrium in engen Kanälen und deren Anwendung auf schnelle Reaktoren.
KFK-Ext. 8/72-1 (Februar 72)

/4/ J. Aberle, A.J. Brook, W. Peppler, H. Rohrbacher, K. Schleisiek:
Sodium Boiling Experiments in a 7-pin-bundle under Flow Run-down Conditions; KFK 2378 (Nov. 1976)

/5/ Y.S. Hoang:
TIGER V, Temperaturberechnung in einem dreidimensionalen System, Programmbeschreibung 234 (1970), unveröffentlicht

/6/ H.K. Fauske:
Transient Liquid Metal Boiling and Two-Phase Flow.
Internat. Seminar on Heat Transfer in Liquid Metals, Trogir/Jugoslawien, 6.-11. Sept. 1971

/7/ K.H. Spiller, D. Perschke, G. Grass:
Messungen der Restfilmstärke bei der Einzelblasenejektion von flüssigem Natrium in einem Rohr.
ATKE 14-21 (1969) 113-117

Condition	SNR		NSK	
	velocity m/s	Δp Pa	velocity m/s	Δp Pa
Stationary	4.5	$4.5 \cdot 10^5$	5.0	$\approx 2 \cdot 10^5$
Onset of boiling	1.25	$0.6 \cdot 10^5$	1.5	$\approx 0.25 \cdot 10^5$

Tab. 1: Comparison of total pressure drop in the SNR 300 between the lower and upper plenum and the NSK test section (including throttling valve).

Run No 16/	Cover gas pressure p_G 10^5 Pa	Heat flux q W/cm^2	Power per unit volume of coolant channel P_v W/cm^3	Steady-state velocity v_2 m/s	Vel. v_2 at the onset of boiling m/s
11	0.785	99	637	≈5	0.52
12	0.785	99	637	≈3	
13	0.785	99	637	≈3	1.25
14	0.785	123	790	4.7	1.10
15	1.18	123	790	≈5	1.3
16	1.18	149	946	≈5	1.85
17	1.18	180	1157	≈5	2.40
20	1.18	149	946	5.05	1.20
21	1.18	149	946	≈5	
22	1.18	180	1157	5.2	2.25
23	1.57	149	946	5.15	0.75
24	1.57	180	1157	5.0	1.55
25	1.57	213	1368	5.05	2.15

Tab. 2: Compilation of the experiments done

Run No.	Heat flux q W/cm^2	Initial velocity v_l m/s	Start of flow reduction s	Onset of boiling t_s s	Time of flow reversal s	Bubble No.	Velocity v_l at t_s m/s	Axial coordinate s m	Local pressure p_s 10^5 Pa	Saturation temperature $T_s = f(p_s)$ °C	Inner wall local surface temperature T_w °C	Boiling superheat $\Delta T_s = T_w - T_s$ K	Superheat acc. Eq.(1) $\Delta T_s = f(\Delta p_u)$ K	Time of max. acceleration s
14	123	4.88	3.00	7.47	8.04	1	1.05	0.48	0.878	866	863	(<0)	23	7.52
				7.66		2		0.49	0.876	866	881	15	40	7.69
				7.83		3		0,48 (?)*	-	-	-	-	50	7.84
				7.92		4		0.35	0.861	863	863	0	39	8.03
20	149	4.88	1.75	6.96	7.06	1	1.15	0.48	1.283	908	923	15	29	7.00
22	180	5.08	2.10	5.72	6.25	1	2.10	0.48	1.305	910	906	(<0)	19	5.75
				5.86		2		0.47	1.327	912	918	6	35	5.88
23	149	5.00	1.25	7.24	7.29	1	0.72	0.33	1.673	939	964	25	53	7.32
24	180	4.85	1.25	5.48	5.80	1	1.50	0,48 (?)*	-	-	-	-	17	5.51
				5.74		5		0.47	1.67	940	966	26	25	5.75
25	213	4.85	2.10	5.79	6.22	1	2.10	0,48 (?)*	-	-	-	-	14	5.80
				5.89		2		0.47	1.690	941	943	2	20	5.91
				6.20		3		0.42	-	-	- *	-	38	6.23

* cannot be estimated with enough certainty

Table 3: Important parameters at the onset of bubble formations

Run No.	Thermo-element	Time section s	Time difference Δt s	Temperature decrease in the wall °C	ΔT K	Effective film thickness S Eq.(3) mm	TIGER cal. mm
	I	8.03 → 8.10	0.07	924 → 918	= 6	0.048*	0.05
	I	8.20 → 8.36	0.16	933 → 906	= 27	0.144	0.15
	L	8.49 → 8.60	0.11	927 → 915	= 12	0.083	
14	I	8.69 → 8.82	0.13	932 → 918	= 14	0.097	
	M	8.79 → 8.89	0.10	922 → 909	= 13	0.083	
	M	9.03 → 9.10	0.07	925 → 917	= 8	0.054	
	N	8.78 → 8.88	0.10	931 → 918	= 13	0.082	
	O	8.78 → 8.87	0.09	918 → 913	= 5	0.054	
20	I	7.05 → 7.17	0.12	943 → 929	= 14	0.105*	0.11
		7.30 → 7.35	0.05	1038 → 1033	= 5	0.045*	
	I	7.44 → 7.51	0.07	1044 → 1025	= 19	0.099	0.12
23	I	7.58 → 7.66	0.08	1033 → 1017	= 16	0.095	
	N	8.35 → 8.44	0.09	1020 → 1014	= 6	0.070	
24	I	5.82 → 6.00	0.18	989 → 967	= 22	0.181*	
	N	6.60 → 6.67	0.07	1004 → 999	= 5	0.063	

* Primary ejection

Tab. 4: Effective Film Thickness according Eq. (3) and TIGER calculation, respectively.

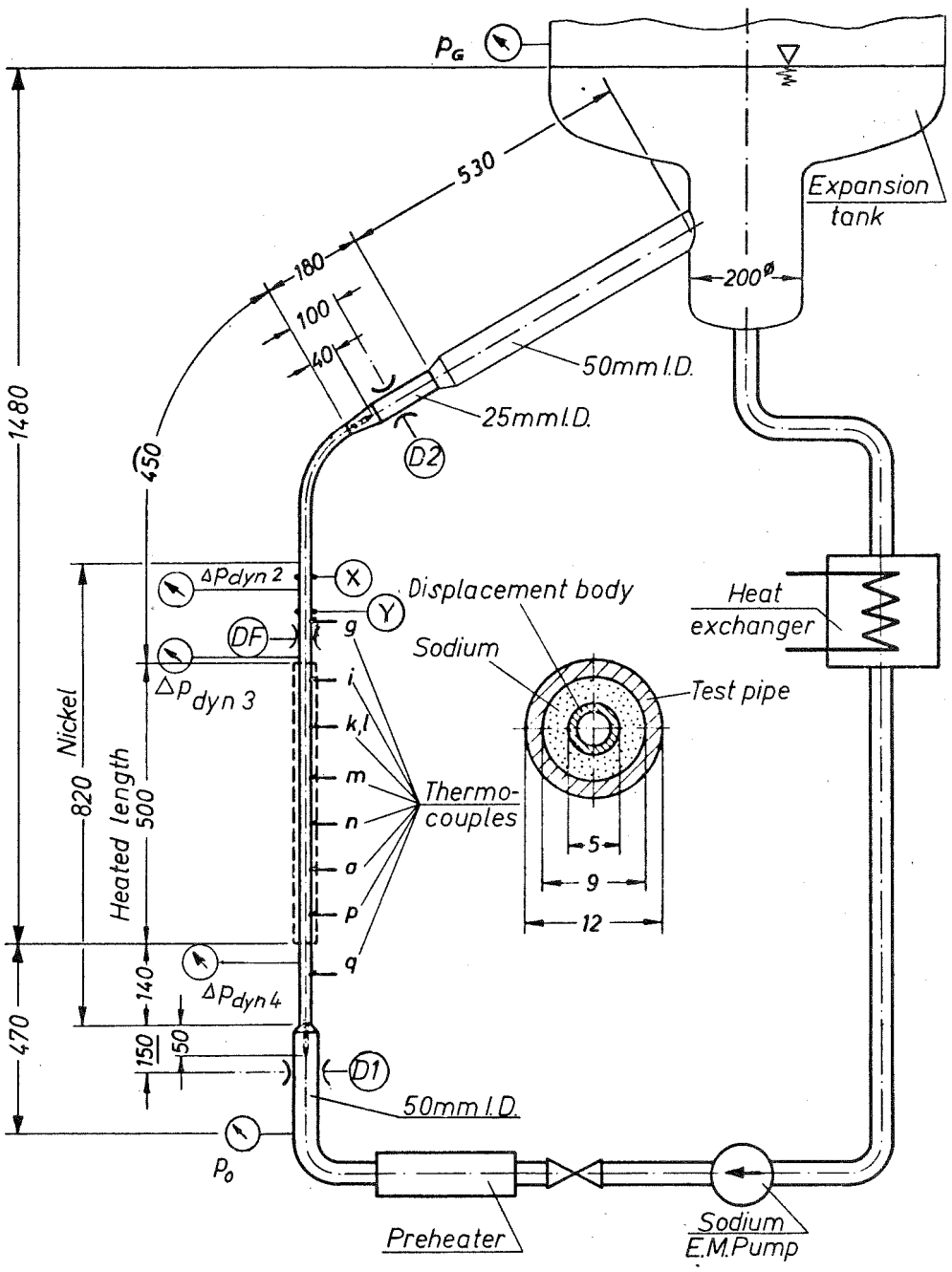

GfK IRE	Test Loop and Test Section, Schematical Arrangement	Fig.1
		17.2.77 Will.

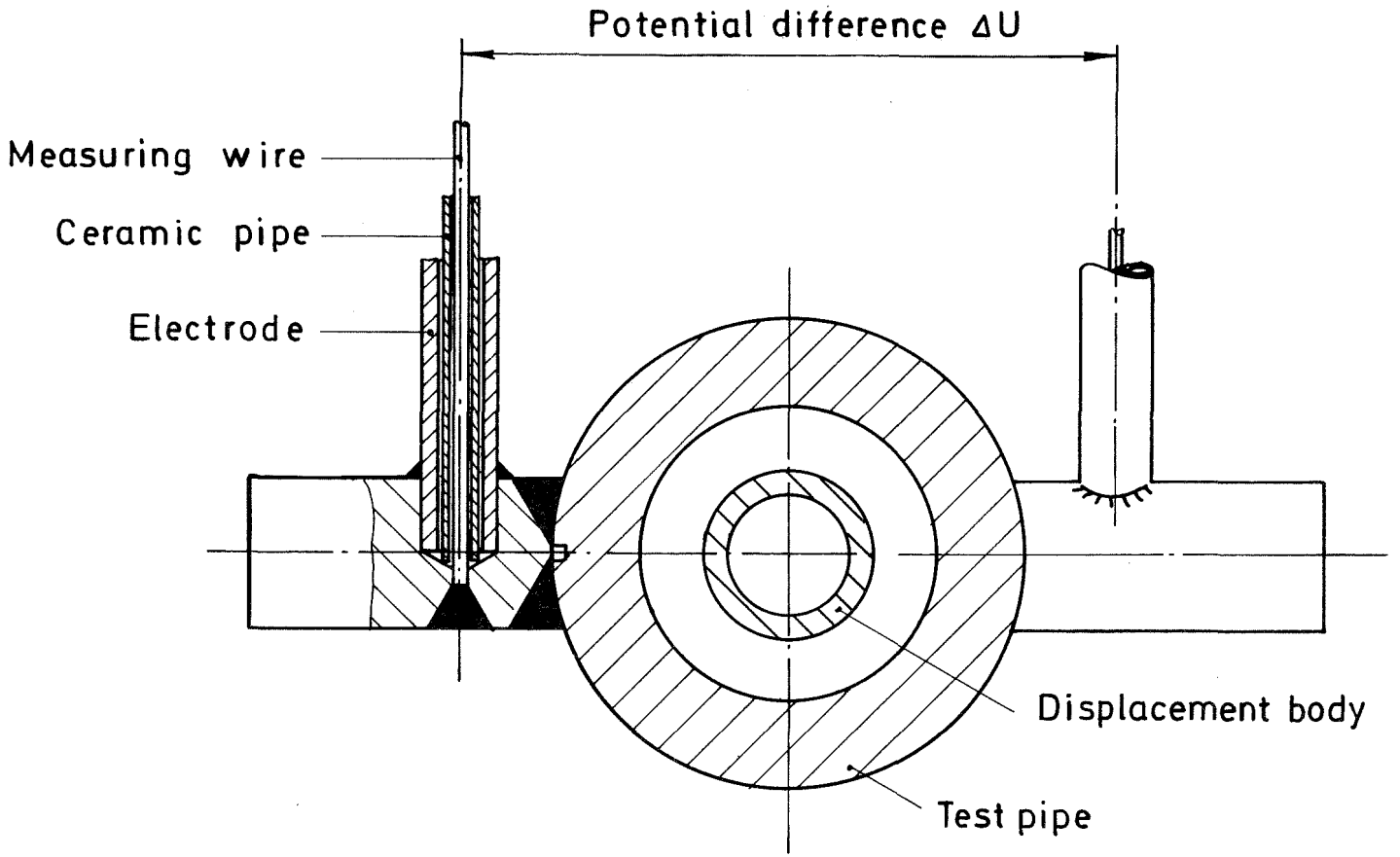

GfK IRE	Bubble Detector (JODEL Principle), Schematical Arrangement	Fig. 2
		17.2.77. Will

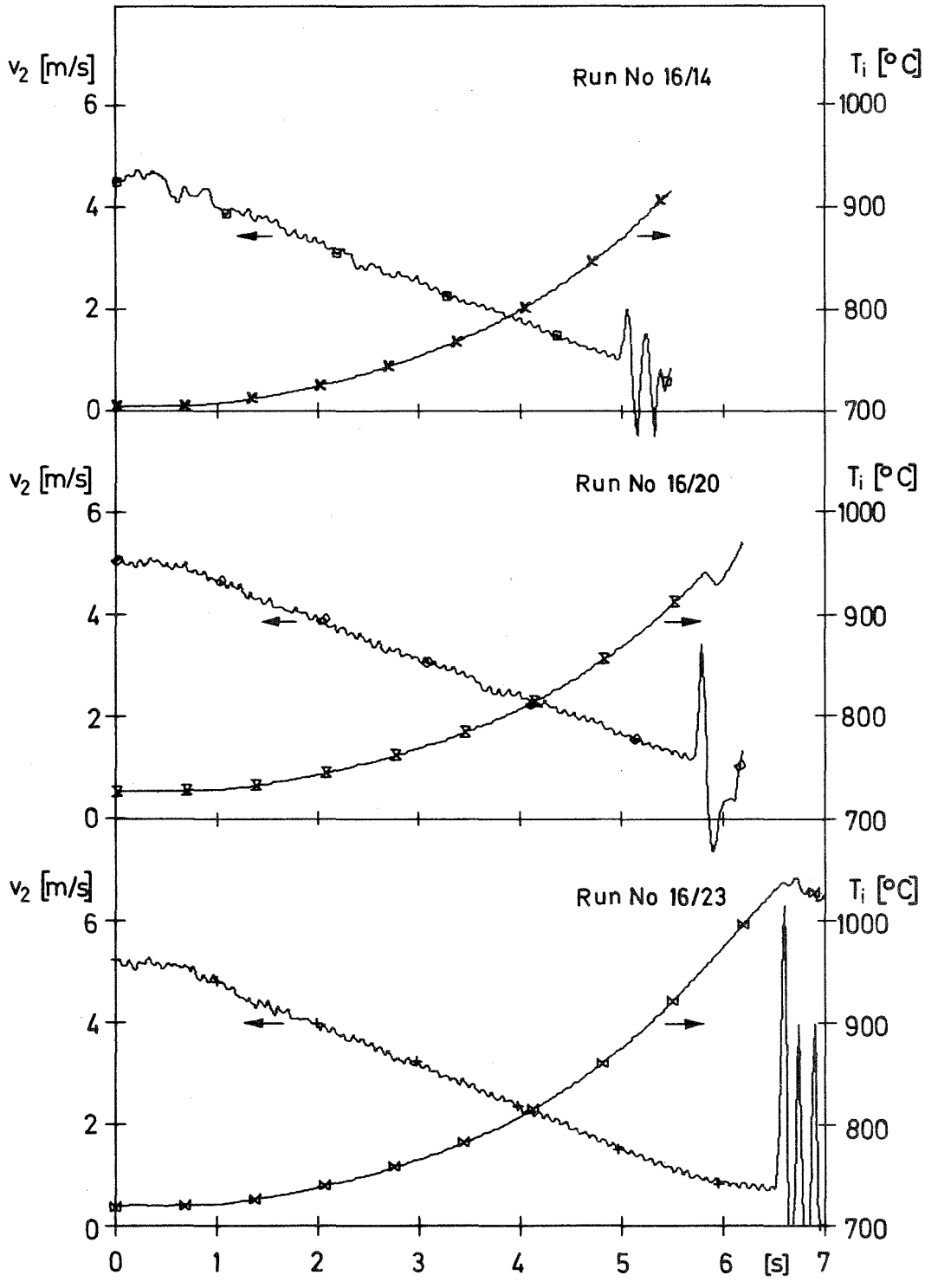

GfK IRE	Flow Rundown Characteristic, Runs No 16/14, 16/20, 16/23	Fig. 3

17.2.77 Will

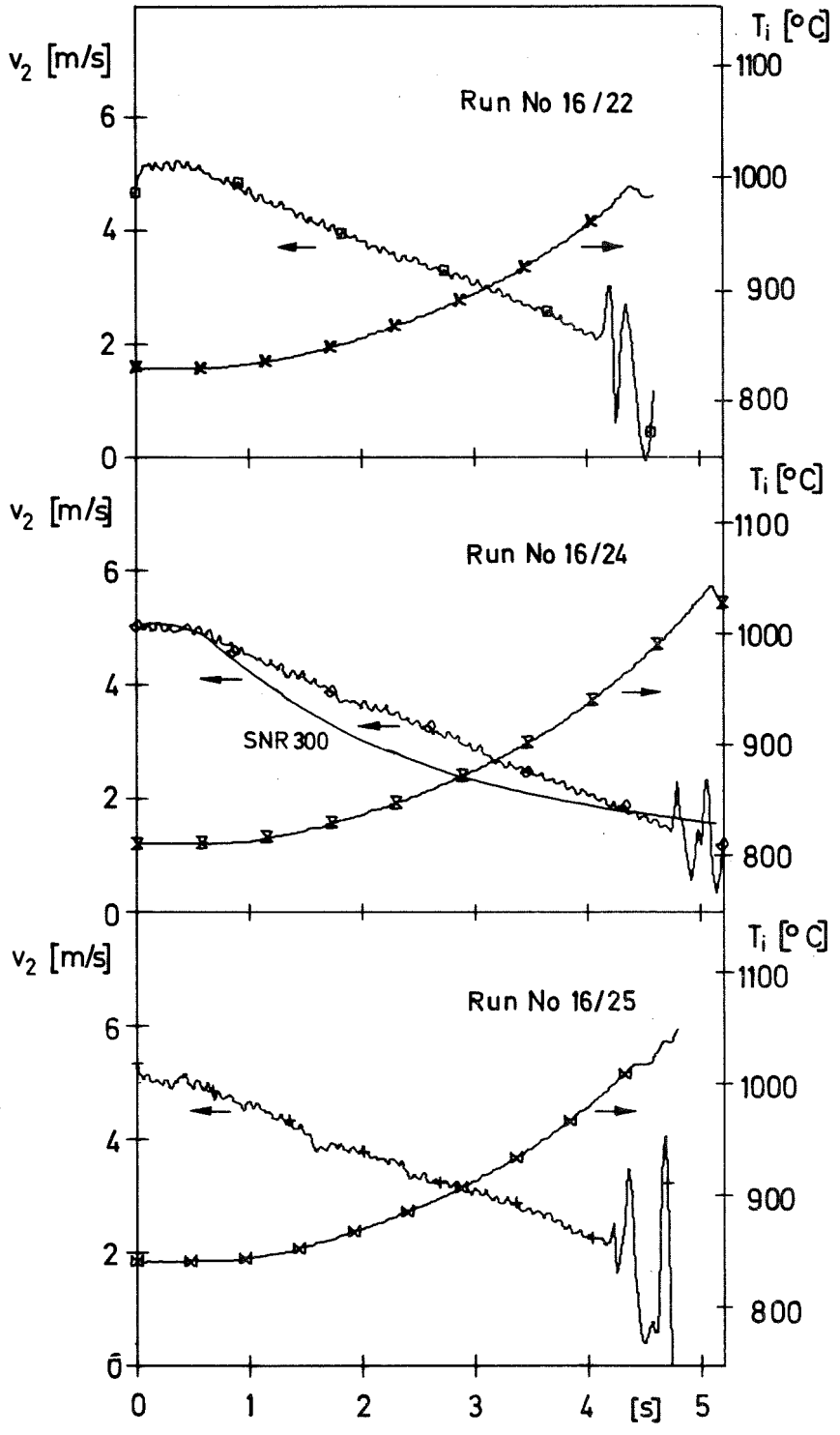

GfK IRE	Flow Rundown Characteristic, Runs No 16/22, 16/24, 16/25	Fig. 4

17.2.77 Will

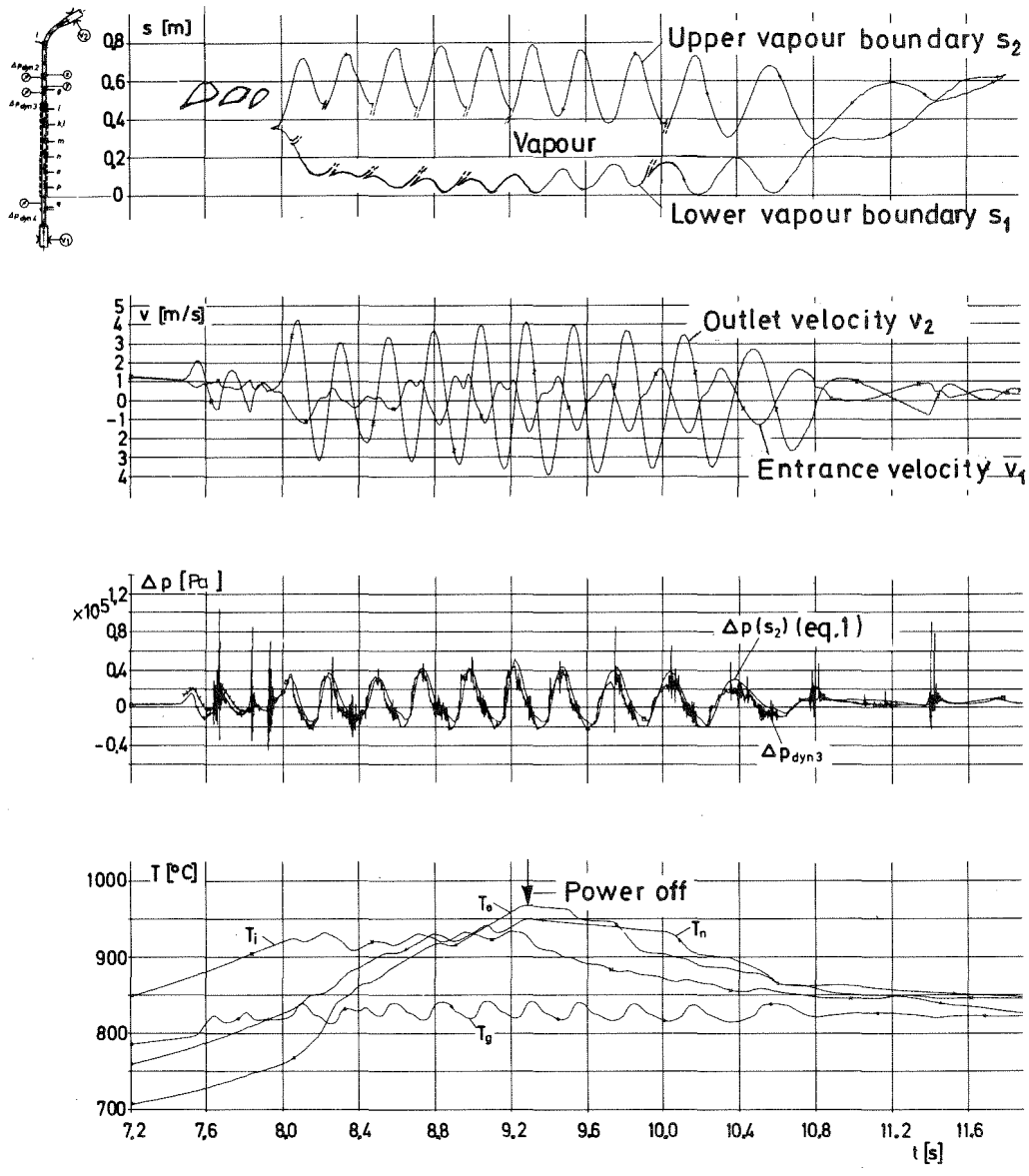

Test parameters:

Heat flux $q = 123\ W/cm^2$

System pressure $p_G = 0.784 \cdot 10^5$ Pa

Initial boiling superheat (acc. eq.(1)) $\Delta T_s = 23$ K

GfK IRE	Transient Boiling under Pump Rundown Conditions, Run No 16/14	Fig. 5
		17.2.72 Will

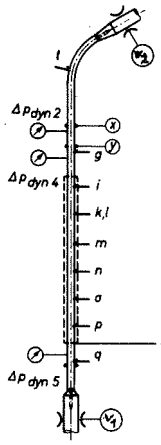

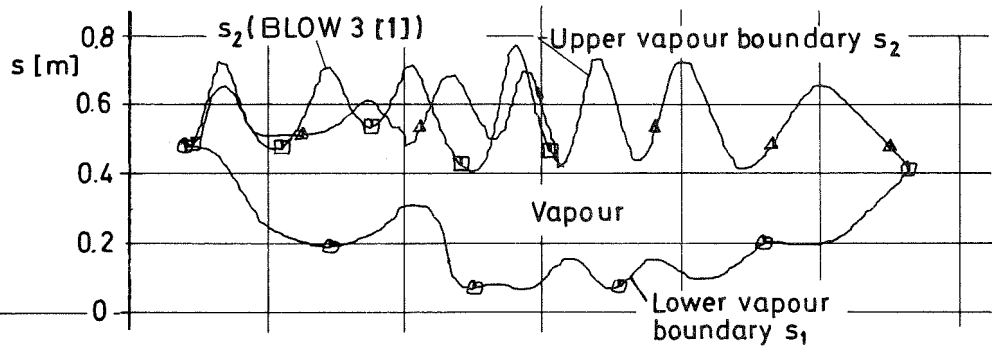

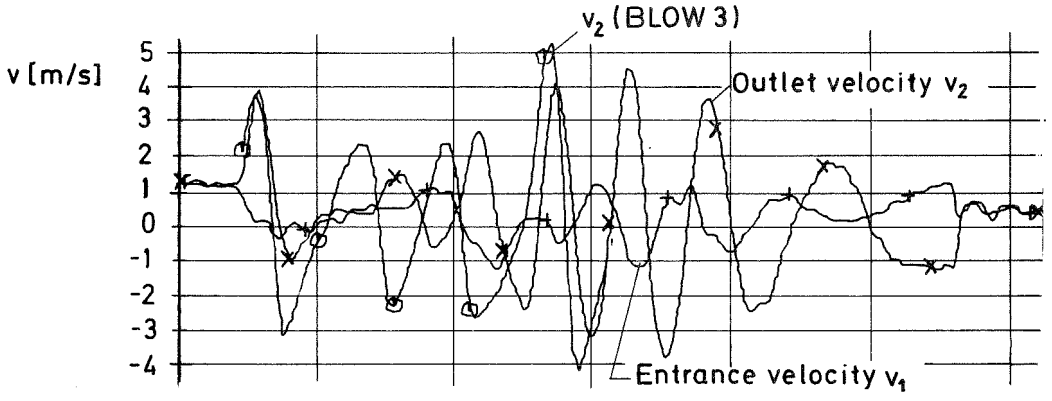

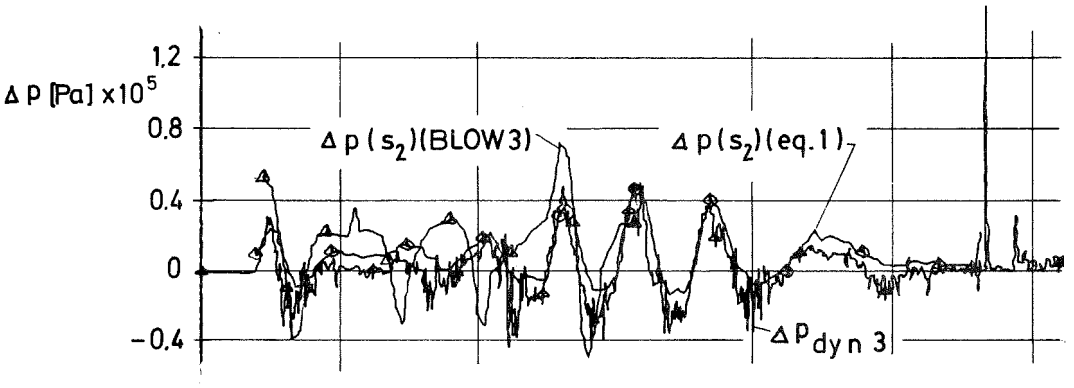

Test parameters:

Heat flux $q = 149\ W/cm^2$

System pressure $P_G = 1.18 \cdot 10^5\ Pa$

Initial boiling superheat $\Delta T_s = 29\ K$ (acc. eq. (1))

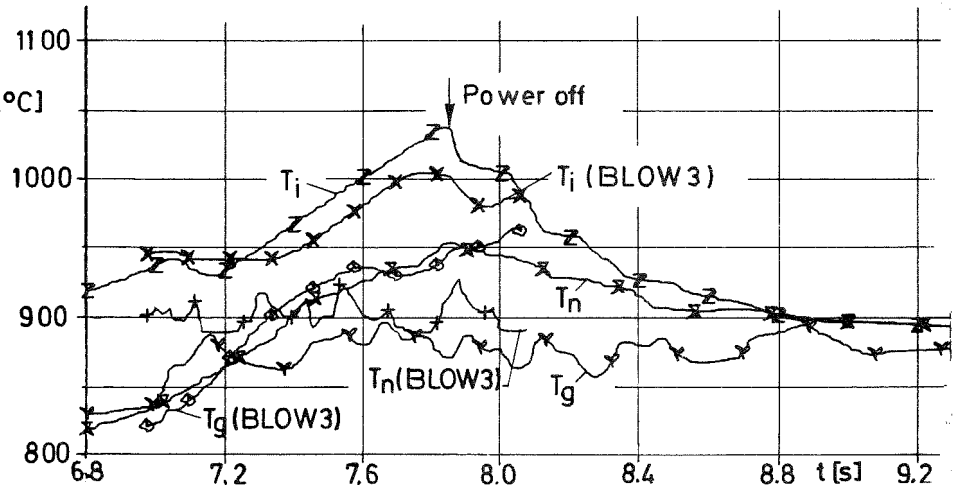

GfK IRE	Transient Boiling under Pump Rundown Conditions Run No 16/20	Fig. 6
		17.2.77 Wil

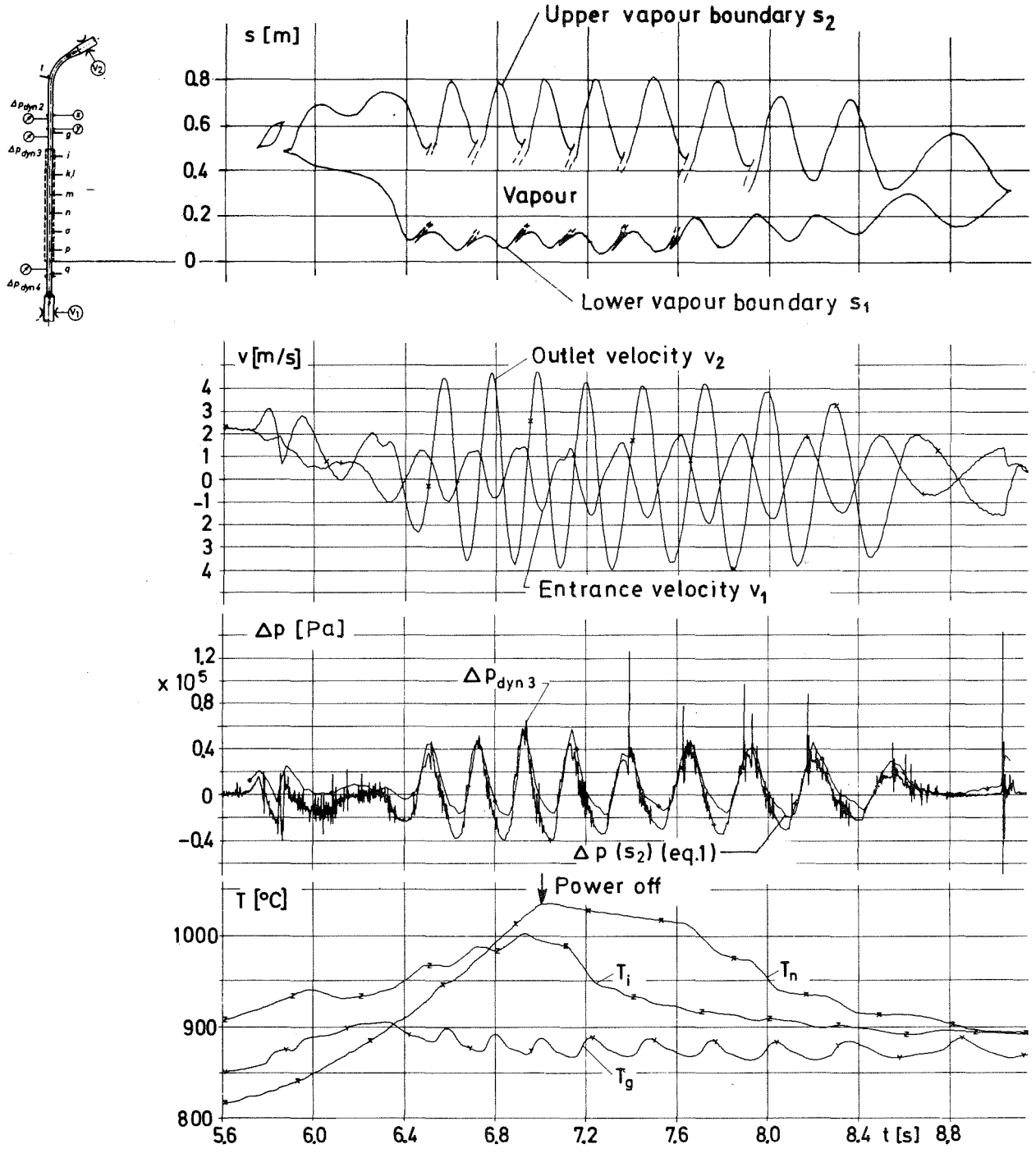

Test parameters:

Heat flux $q = 1.80\,W/cm^2$

System pressure $p_G = 1.18 \cdot 10^5 Pa$

Initial boiling superheat (acc. eq.(1)) $\Delta T = 19\,K$

GfK IRE	Transient Boiling under Pump Rundown Conditions, Run No 16/22	Fig. 7
		17.2.77 Will

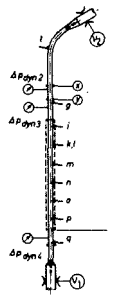

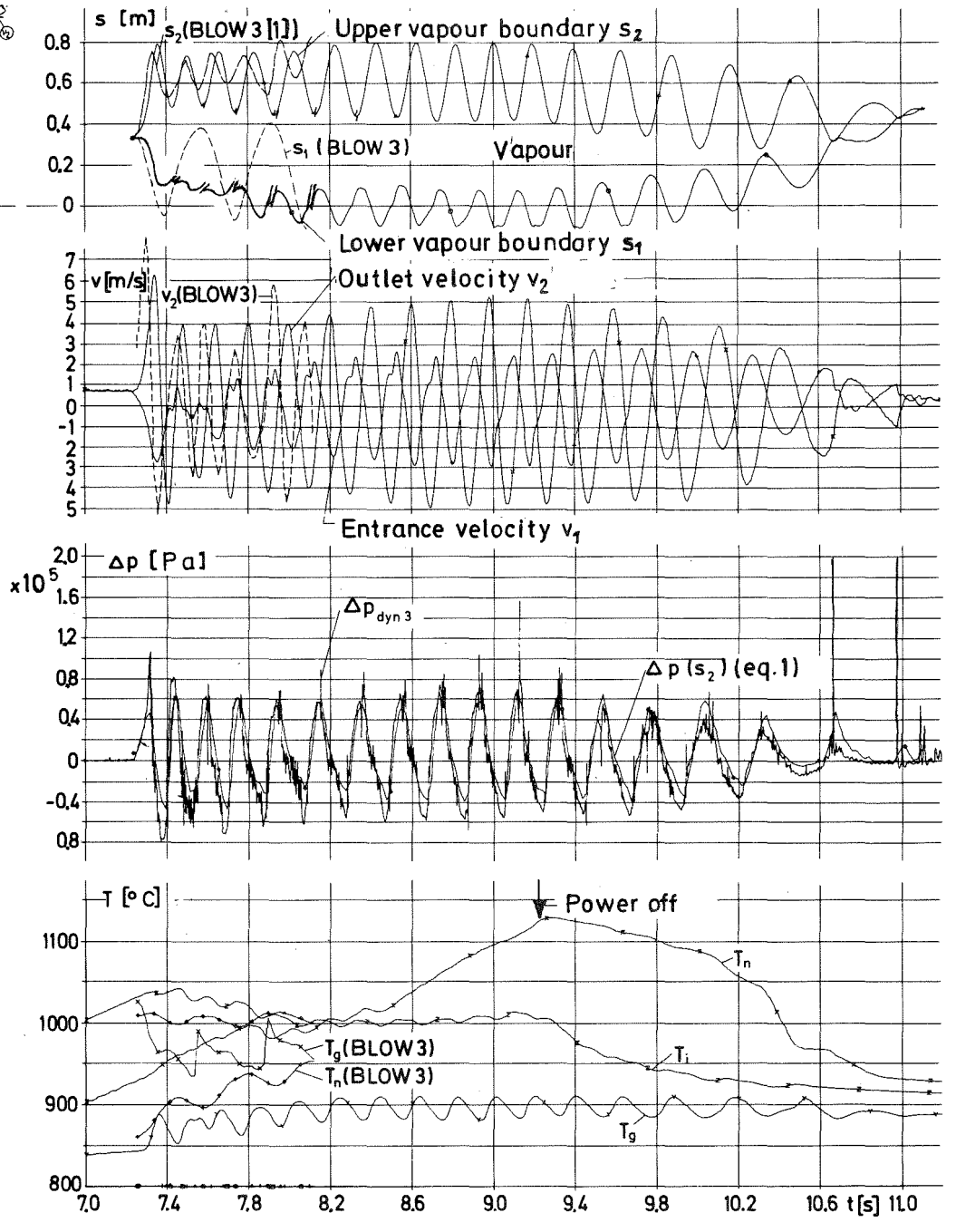

Test parameters:

Heat flux $q = 149\ W/cm^2$

System pressure $p_G = 1.57 \cdot 10^5\ Pa$

Initial boiling superheat (acc. eq.(1)) $\Delta T_s = 53\ K$

GfK IRE	Transient Boiling under Pump Rundown Conditions, Run No 16/23	Fig. 8
		17.2.77 Will

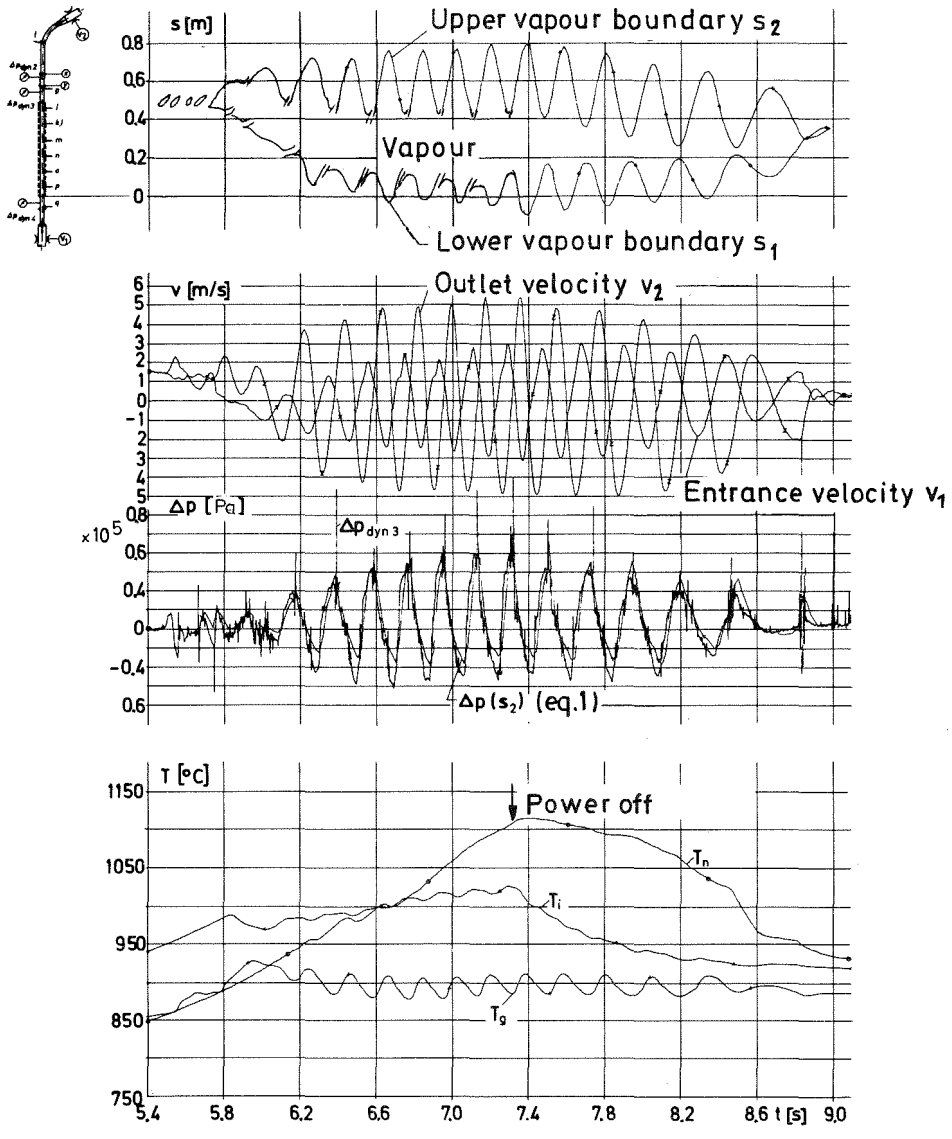

Test parameters:

Heat flux	$q = 180\ W/cm^2$
System pressure	$p_G = 1.57 \cdot 10^5\ Pa$
Initial boiling superheat (acc. eq.(1))	$\Delta T_S = 17\ K$

GfK IRE	Transient Boiling under Pump Rundown Conditions, Run No 16/24	Fig. 9
		17.2.77 Will

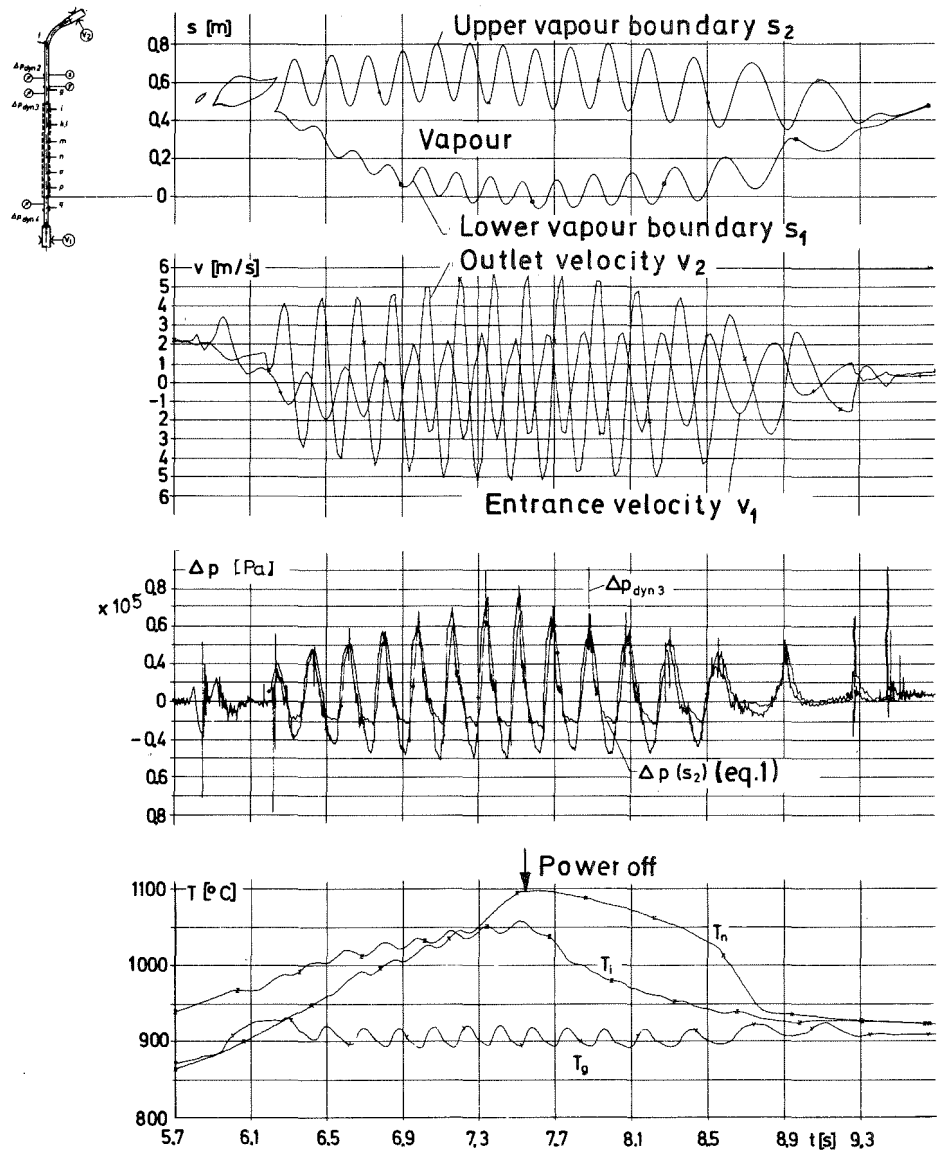

Test parameters:

Heat flux $q = 213\ W/cm^2$

System pressure $P_G = 1.57 \cdot 10^5\ Pa$

Initial boiling superheat (acc. eq.(1)) $\Delta T_s = 14\ K$

GfK IRE	Transient Boiling under Pump Rundown Condition, Run No 16/25	Fig. 10
		17.2.77 Will

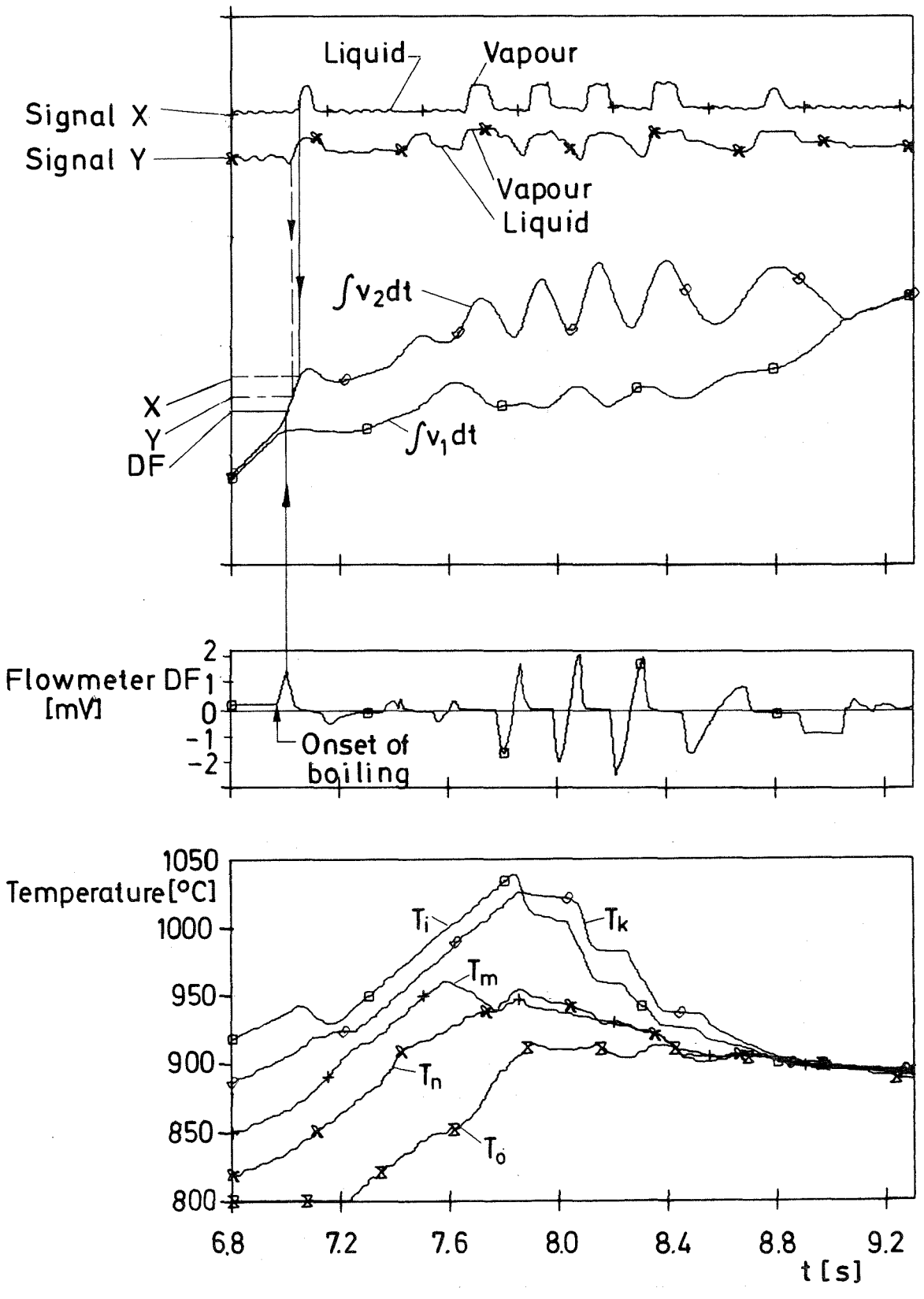

GfK IRE	Sample Signals Used for Evaluation of the Void Pattern Run No 16/20	Fig.11
		17.2.77 Will

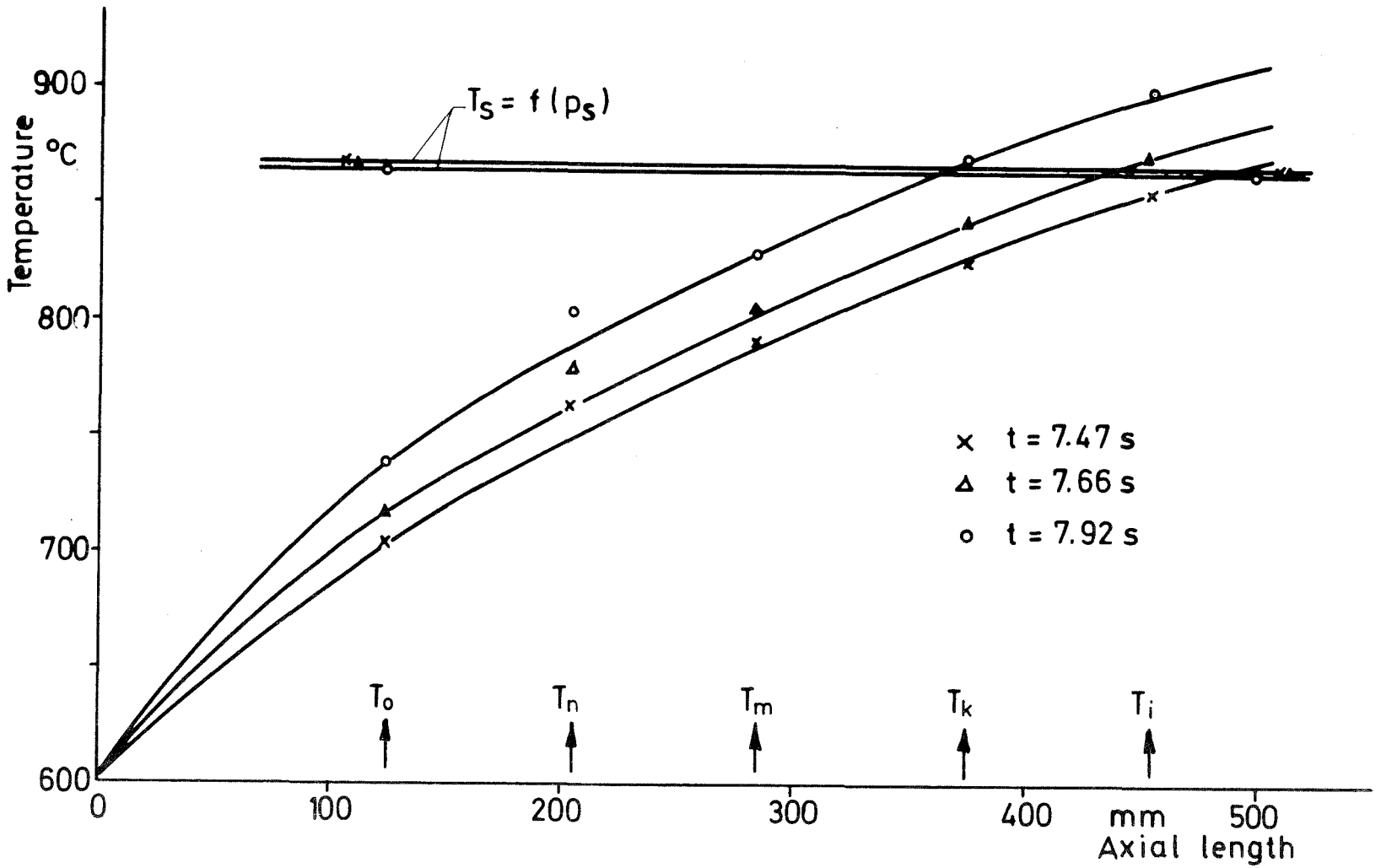

GfK IRE	Axial Temperature Distribution at the Inner Wall Surface Run No 16/14	Fig. 12
		12.2.73 Will

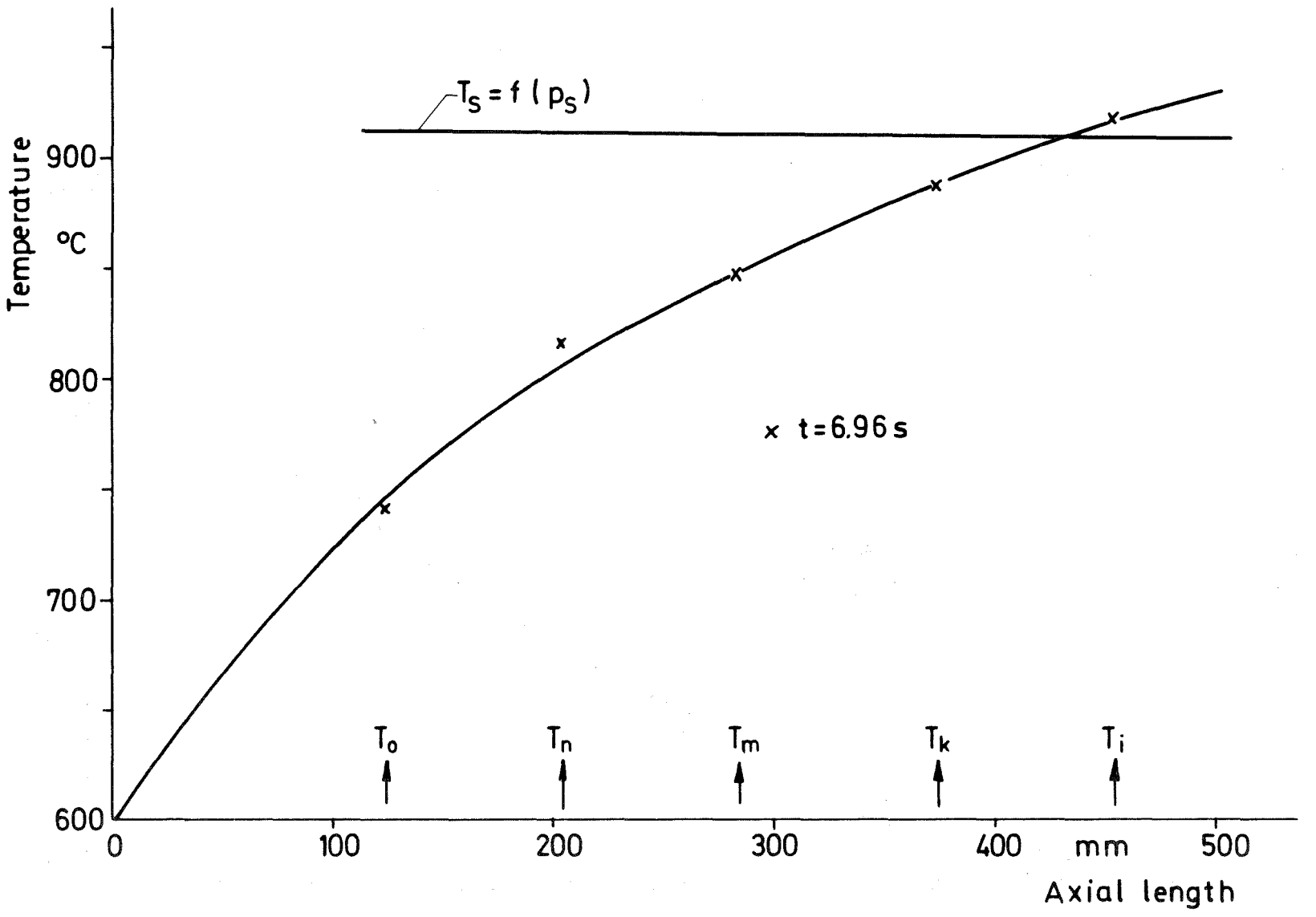

GfK IRE	Axial Temperature Distribution at the Inner Wall Surface Run No 16/20	Fig. 13
		17.2.77 Will

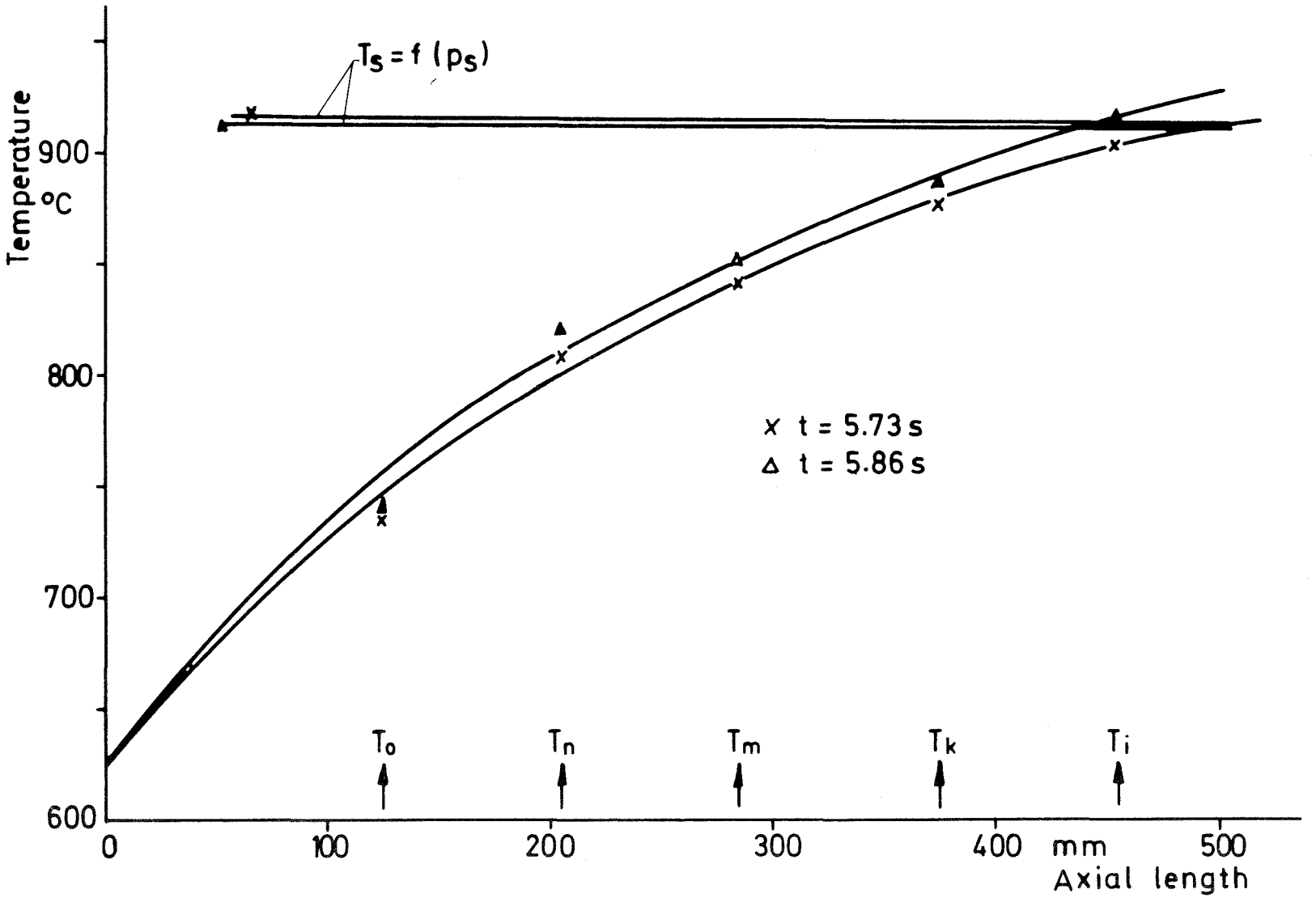

GfK IRE	Axial Temperature Distribution at the Inner Wall Surface Run No 16/22	Fig. 14

12.2.77 Will

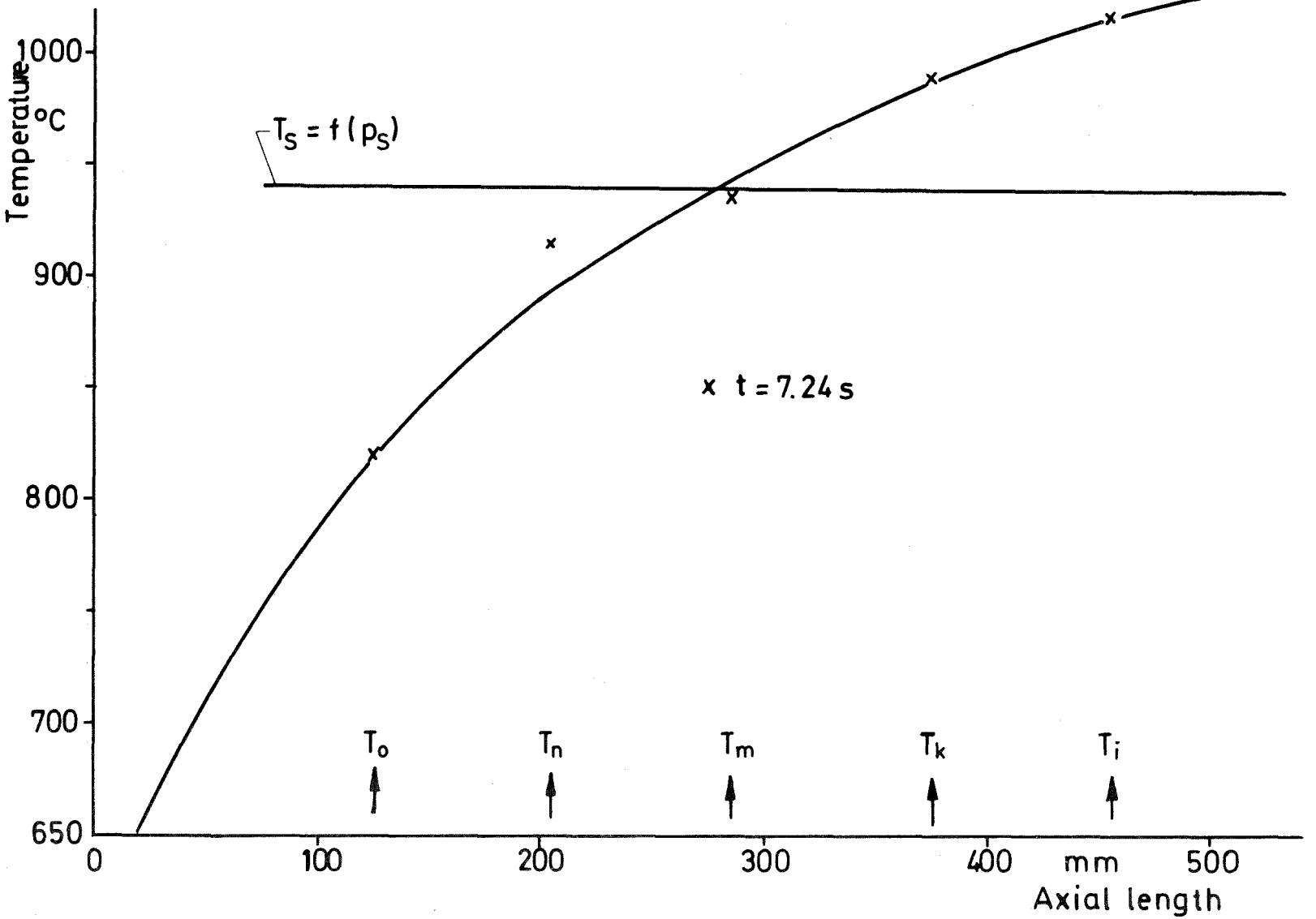

GfK IRE	Axial Temperature Distribution at the Inner Wall Surface Run No 16/23	Fig. 15
		18.2.77 Will

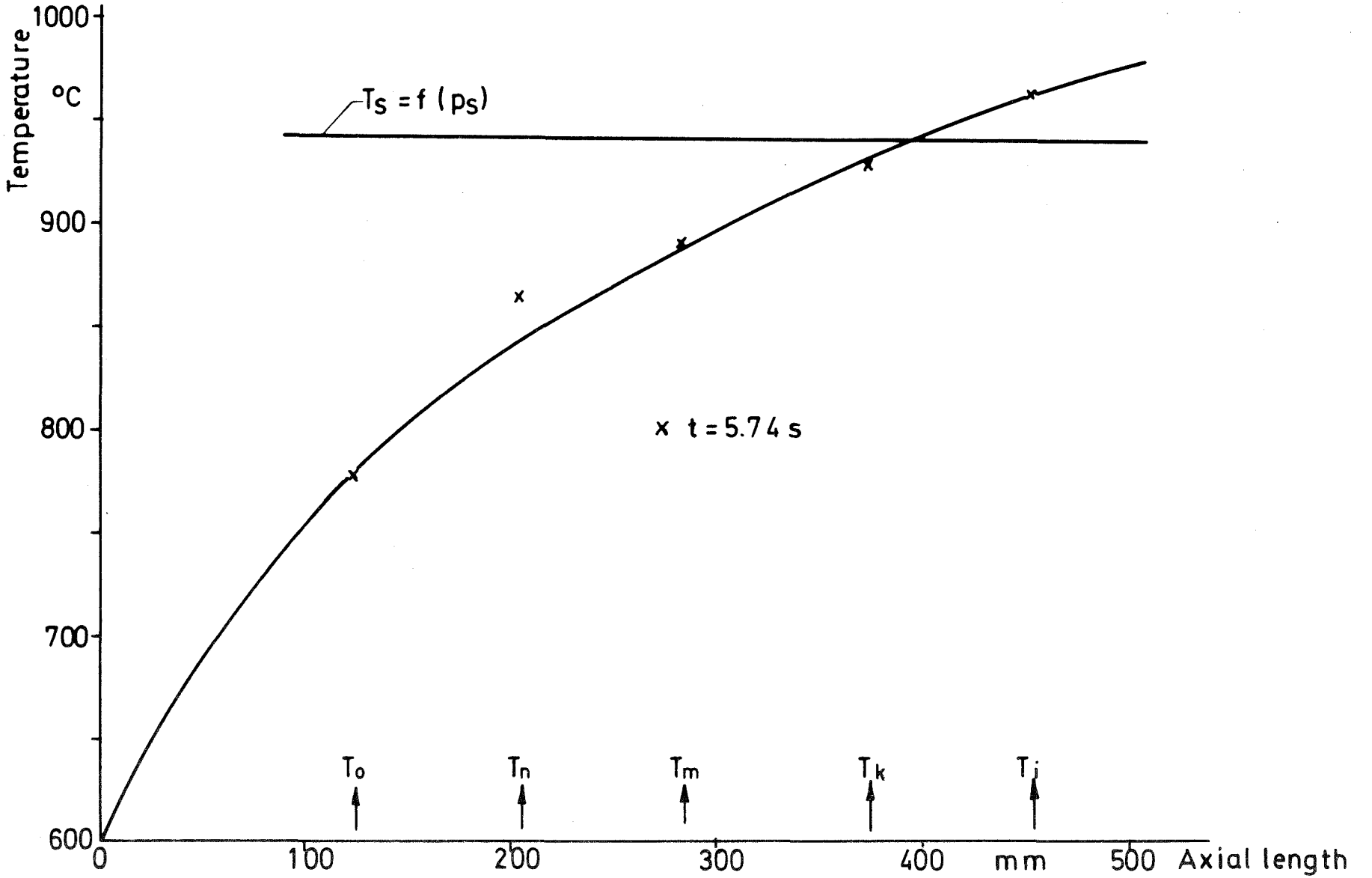

GfK IRE	Axial Temperature Distribution at the Inner Wall Surface Run No 16/24	Fig. 16
		17.2.70 Wil

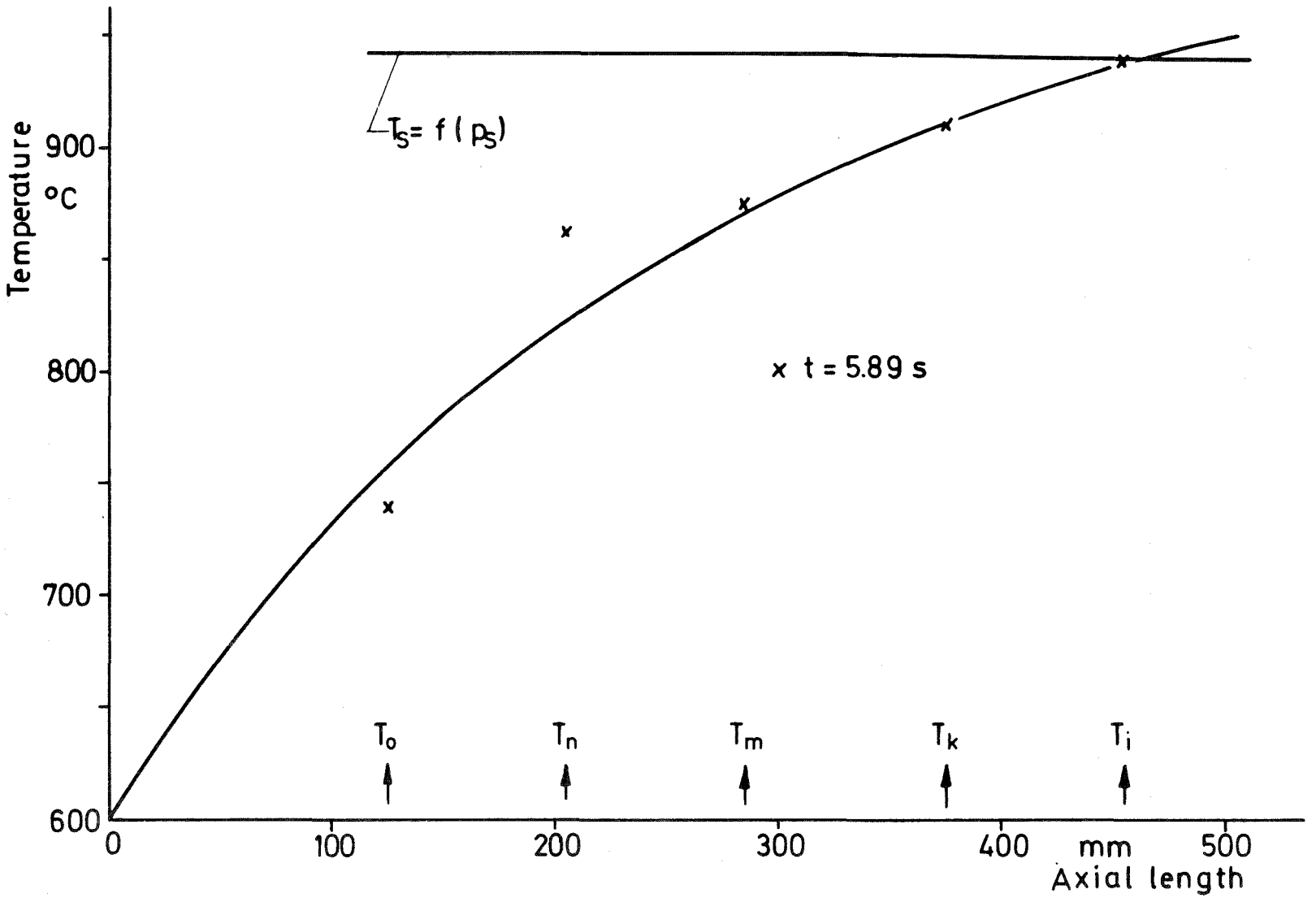

GfK IRE	Axial Temperature Distribution at the Inner Wall Surface Run No 16/25	Fig. 17

17.2.77 Will

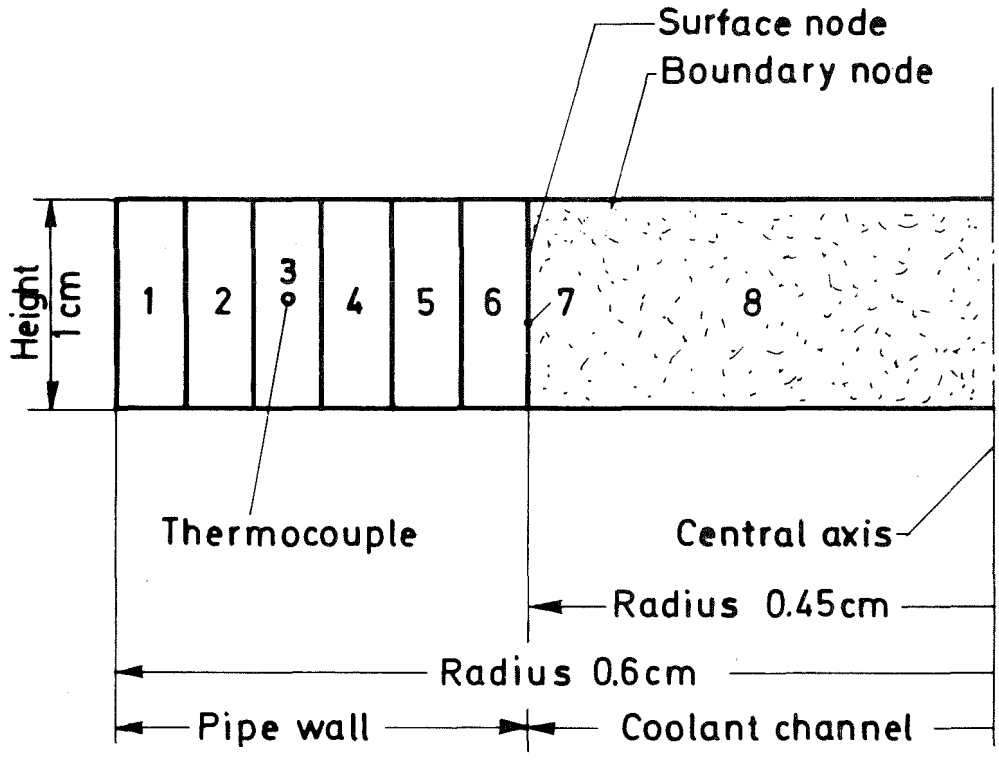

GfK IRE	Calculational Mesh Used in TIGER-Calculation	Fig. 18
		17.2.77

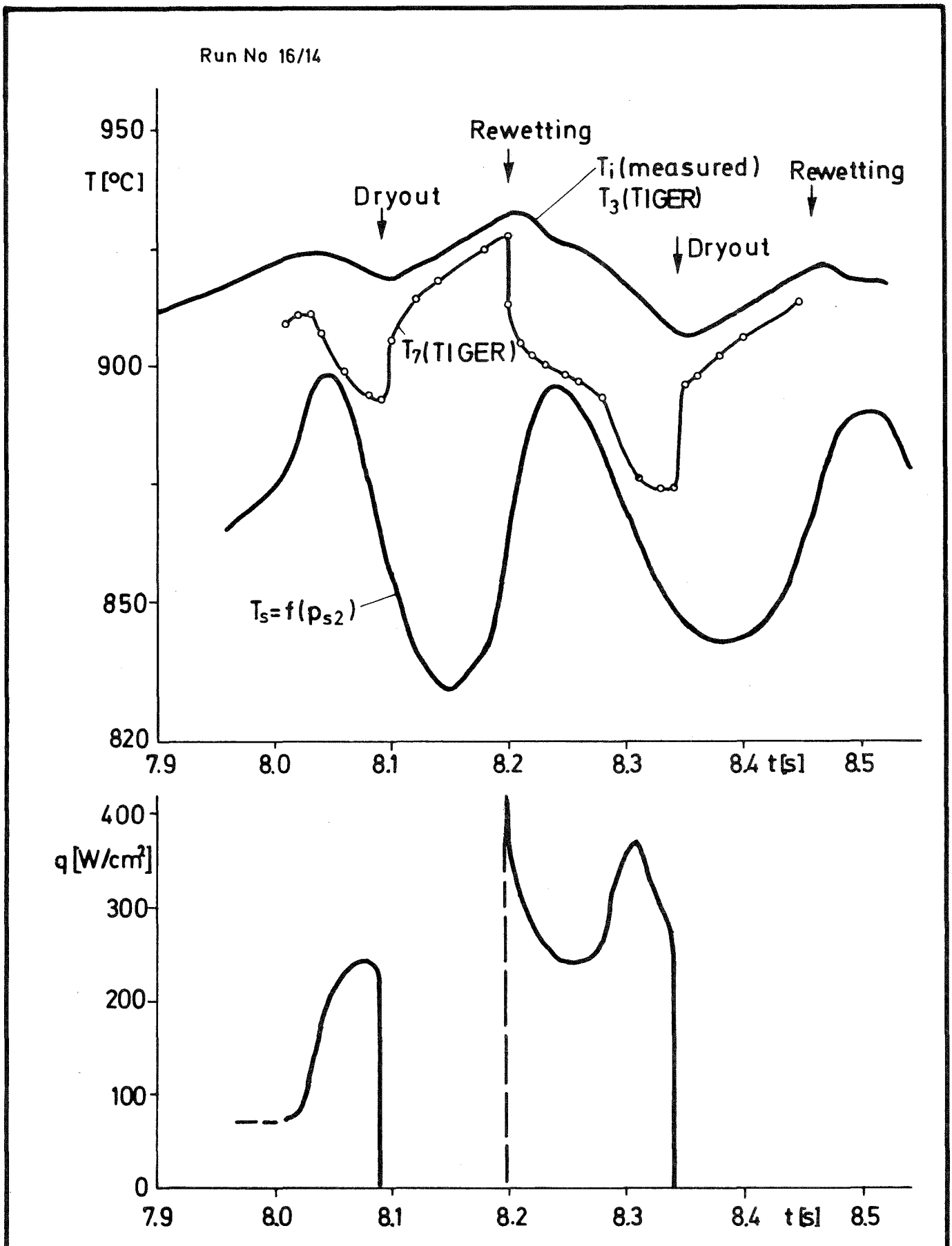

GfK IRE	Heat Flux and Course of Temperature during Film Evaporation	Fig. 19

17. 2. 77 Hil